Tectonophysics 626 (2014) 41–52

Contents lists available at ScienceDirect

Tectonophysics

journal homepage: www.elsevier.com/locate/tecto

Evolution of the Eastern Karakoram Metamorphic Complex, Ladakh, NW India, and its relationship to magmatism and regional tectonics

David Wallis *, R.J. Phillips, G.E. Lloyd

School of Earth and Environment, University of Leeds, Leeds LS2 9JT, UK

ARTICLE INFO

Article history:
Received 22 January 2014
Received in revised form 24 March 2014
Accepted 26 March 2014
Available online 2 April 2014

Keywords:
Karakoram
Fault
Metamorphic
Evolution
Crustal
Leucogranite

ABSTRACT

The eastern Karakoram terrane, NW India, records crustal evolution in the core of the Himalayan–Tibetan orogen. Recent debate has centred on whether prograde metamorphism, anatexis and leucogranite emplacement were the result of localised shear heating and magma advection within the Karakoram Fault Zone (KFZ) or instead predate the KFZ and were the result of regional tectonometamophic events. Inclusions within andalusite porphyroblasts that grew during 15.7 Ma leucogranite emplacement have fabrics that are random or discordant to the KFZ matrix foliation, indicating that the KFZ initiated after this time. Therefore, earlier anatexis and metamorphism are the result of regional metamorphic events. Amphibole–plagioclase thermobarometry on a c. 17 Ma migmatite melanosome, later exhumed within a transpressional zone of the KFZ, shows that melting occurred at 688 °C and 522 MPa. Amphibolites record an older kyanite-grade metamorphic event that occurred at 677–736 °C and 875–1059 MPa. Metapelites also record a kyanite-grade event which is constrained by Ti-in-biotite thermometry to have occurred at 622 °C and >650 MPa. The tectonometamorphic history of the eastern Karakoram correlates closely with that of the central Karakoram away from the KFZ. This correlation supports the interpretation that metamorphism and anatexis were regional in extent and also indicates a limited offset of <150 km on the KFZ.

© 2014 The Authors. Published by Elsevier B.V. This is an open access article under the CC BY license (http://creativecommons.org/licenses/by/3.0/).

1. Introduction

Understanding the evolution of the continental crust during the orogenic cycle, the pressure–temperature paths experienced by metamorphic rocks and their relationship to magmatic and deformation processes are fundamental but challenging issues. The complex histories of rocks in continental collision zones must be deciphered to place constraints on the evolution of an orogen. The Karakoram–Qiangtang terrane in the Himalayan–Tibetan orogen (Fig. 1a) provides an opportunity to investigate the former south Asian active margin, which later became the core of the orogen, and hence holds key information on crustal evolution in these tectonic settings. The Karakoram terrane in Pakistan is relatively well studied and has yielded much information on its complex history (e.g. Foster et al., 2004; Fraser et al., 2001; Palin et al., 2012; Villa et al., 1996). However, surface exposures of its correlative, the Qiangtang terrane in Tibet, consist predominantly of supracrustal and early Mesozoic metamorphic lithologies, which record little information on mid- to lower-crustal processes around the time of India–Asia collision (Pullen et al., 2011). The eastern Karakoram in Ladakh, NW India, geographically links the central Karakoram with the Qiangtang terrane and contains exposures of basement lithologies exhumed from a range of depths. However, metamorphism in this region remains relatively less studied and has potential to further our understanding of these key terranes.

The Karakoram terrane in the Hunza and Baltoro regions of Pakistan has experienced five metamorphic events (M_0–M_4). M_0 is represented in Hunza by Early Cretaceous andalusite-grade contact metamorphism during subduction prior to closure of the Shyok suture (Palin et al., 2012). Late Cretaceous closure of the Shyok suture resulted in regional sillimanite-grade M_1 metamorphism in Hunza, culminating in Eocene migmatisation following closure of the Indus suture during India–Asia collision (Foster et al., 2004; Fraser et al., 2001). Oligo-Miocene kyanite-grade M_2 metamorphism in Hunza and Baltoro was closely followed by an M_3 staurolite-grade event during the mid-Miocene in Hunza (Fraser et al., 2001; Palin et al., 2012; Villa et al., 1996). M_4 Mio-Pliocene sillimanite-grade metamorphism is represented by migmatisation in the Bullah and Dassu domes in the Baltoro (Fraser et al., 2001).

In the eastern Karakoram, the Karakoram Fault Zone (KFZ) cuts through medium-high grade metamorphic rocks of the Karakoram terrane and is spatially associated with exposed migmatite and large volumes of leucogranite (Phillips, 2008). Recent debate has centred on whether prograde metamorphism resulted from shear heating and/or fault-guided magmatic advection within the KFZ (Rolland and Pêcher,

Abbreviations: KFZ, Karakoram Fault Zone; EKMC, Eastern Karakoram Metamorphic Complex; PTZ, Pangong Transpressional Zone; PMC, Pangong Metamorphic Complex.

* Corresponding author.
E-mail address: eedw@leeds.ac.uk (D. Wallis).

http://dx.doi.org/10.1016/j.tecto.2014.03.023
0040-1951/© 2014 The Authors. Published by Elsevier B.V. This is an open access article under the CC BY license (http://creativecommons.org/licenses/by/3.0/).

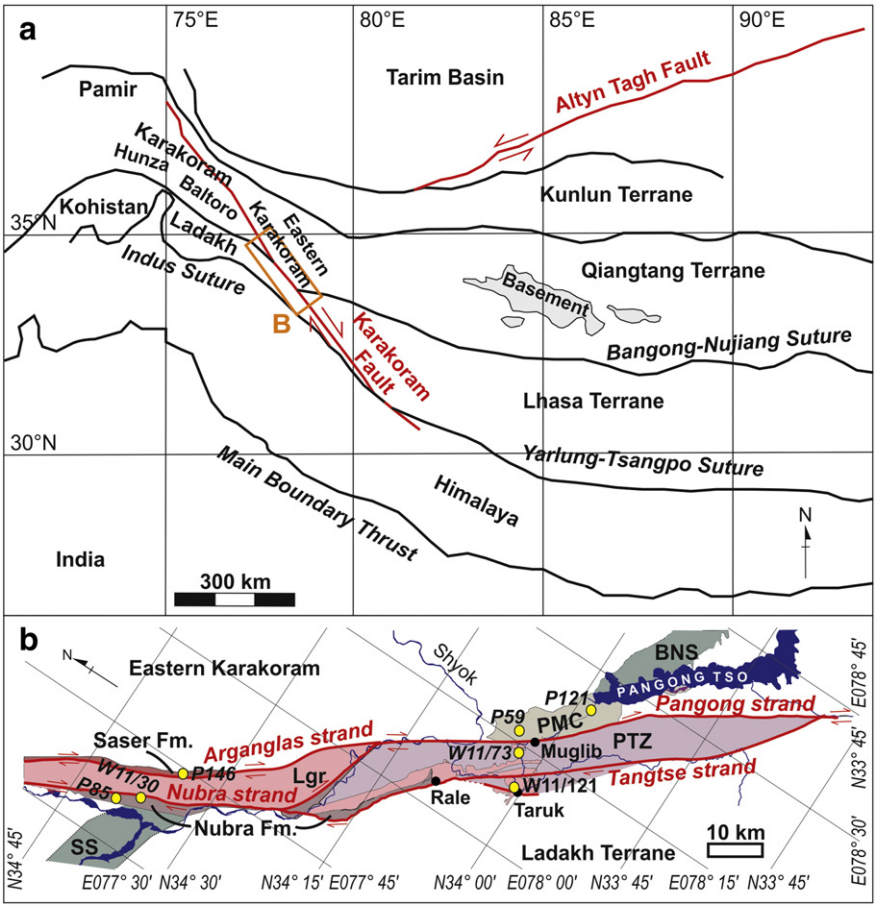

Fig. 1. Location maps. (a) Simplified terrane map of the Himalaya and Tibet showing the location of the Hunza, Baltoro and eastern Karakoram (modified from Searle et al., 2011). Also shown is the extent of basement exposure within the Qiangtang terrane in Tibet (from Pullen et al., 2011). The study area is marked by the orange box and expanded in part (b). (b) The central portion of the Karakoram fault zone in Ladakh, NW India showing the four subunits of the Eastern Karakoram Metamorphic Complex; the Pangong Transpressional Zone (PTZ), Pangong Metamorphic Complex (PMC), Nubra Formation and Saser Formation. Also shown are the major bodies of Miocene leucogranites (Lgr), Bangong–Nujiang sutre (BNS) and Shyok suture (SS). Sample localities are marked in yellow.
Modified from Phillips (2008).

2001; Rolland et al., 2009; Valli et al., 2008), or alternatively was the result of widespread crustal thickening (Searle et al., 1998, 2011; Streule et al., 2009). Rolland and Pêcher (2001) and Rolland et al. (2009) propose that high geothermal gradients within the KFZ demonstrate that it is a lithospheric-scale fault that has generated shear heating and channelled magmas during plate-like extrusion of the Tibetan Plateau. Elevated $^{3}He/^{4}He$ ratios from geothermal springs on the fault have also been put forward as evidence that the KFZ accesses the mantle (Klemperer et al., 2013). However, cross-sections based on shortening estimates across the Himalaya require that the KFZ is confined within the Tibetan crust as it must by underlain by subducted Indian lithosphere for much of its length (Searle et al., 2010). Also, peak metamorphism adjacent to the KFZ predates strike-slip deformation on the fault (Streule et al., 2009) and can be correlated with metamorphic events away from the KFZ in the Hunza region of the Karakoram (Fraser et al., 2001; Palin et al., 2012). Thus, prograde metamorphism throughout the Karakoram may be the result of regionally extensive crustal thickening and magmatism, rather than localised deformation. Wallis et al. (2013) reported that deformation within the KFZ is associated with retrograde metamorphism during exhumation and fluid flux, rather than prograde metamorphism.

The age of the KFZ has also been contested and depends primarily upon the relative ages of the fault and Miocene granitoid intrusions along its length. Interpretations that the intrusions are synkinematic with respect to the KFZ have led some authors to suggest that the KFZ initiated as early as 22–34 Ma (Boutonnet et al., 2012; Lacassin et al., 2004a,b; Leloup et al., 2011, 2013; Valli et al., 2008; Weinberg et al., 2009). These suggestions are based on synkinematic interpretations of outcrop-scale structures or microstructures. However, such interpretations are made more difficult and potentially less reliable by overprinting of high temperature microstructures by later lower temperature deformation fabrics and by the potential for older pre-KFZ outcrop- to micro-scale structures to rotate into alignment with the fault during later deformation. Alternative prekinematic interpretations of the intrusions, based on regional mapping, thermochronology and field and microstructural criteria, have also been put forward as evidence that the KFZ initiated after c. 15.7 Ma and is therefore a significantly more recent structure (Phillips and Searle, 2007; Phillips et al., 2004; Searle, 1996; Wang et al., 2011, 2013a,b). If this is the case then the KFZ cannot have been the cause of anatexis and leucogranite generation between c. 22 and 16 Ma (Phillips et al., 2013). In this contribution we investigate metamorphism throughout the Eastern Karakoram Metamorphic Complex (EKMC) and its relationship to regional and local (i.e. KFZ) tectonic events.

2. The Eastern Karakoram Metamorphic Complex

The EKMC in Ladakh, NW India, makes up the metamorphic country rock of the Karakoram terrane in this region and has been correlated with the Karakoram Metamorphic Complex in the Baltoro and Hunza regions (Fig. 1a) of Pakistan (Searle and Phillips, 2007; Searle et al., 2010; Streule et al., 2009). The EKMC is composed of four sub-units: the Pangong Transpressional Zone (PTZ) and Pangong Metamorphic

Complex (PMC) in the SE and the Nubra and Saser formations in the NW (Phillips, 2008; Phillips and Searle, 2007).

The PTZ (Fig. 1b) is bounded mainly by the Tangtse and Pangong strands of the Karakoram Fault Zone (KFZ) (Phillips et al., 2004) and contains a portion of the Karakoram terrane exhumed by transpressional fault motion (Weinberg and Searle, 1998) (Fig. 2a–c). Within the PTZ, amphibolites, metapelites, psammites and calc-silicates are intruded by I-type Cretaceous diorites–granodiorites, and younger S-type leucogranites associated with Miocene migmatisation (Phillips et al., 2013; Weinberg and Searle, 1998). Prograde metamorphism of the PTZ is recorded by Grt + Ky + St metapelites in which garnets have Mn-rich, Fe-poor cores overgrown by Mn-poor, Fe-rich rims at 680 °C and 850 MPa (Thanh et al., 2011). Rolland and Pêcher (2001) proposed that peak metamorphic granulite facies conditions of >800 °C and c. 550 MPa were attained on the basis of the assemblage Cpx + Prg + Scp + Spl + Qtz + Pl. However, more widely preserved mineral assemblages span upper amphibolite (Fig. 2b) to greenschist facies (Reichardt et al., 2010) and have been suggested to record conditions of 700–750 °C and 400–500 MPa and 350–400 °C and 300–400 MPa respectively (Rolland and Pêcher, 2001; Rolland et al., 2009). Extensive migmatisation of metapelites, Bt-psammites and Cretaceous granodiorites is evident within the PTZ (Fig. 2a). Reichardt et al. (2010) proposed that this anatexis occurred at 675–750 °C and 600–800 MPa by the reaction Bt + Pl + Qtz + fluid = Hbl + melt ± Kfs. Migmatisation of the currently exposed structural level occurred at c. 17.4 M, whilst leucogranitic dykes and plutons in the PTZ span 22–13 Ma (Phillips et al., 2013). The retrograde path of the PTZ is constrained by $^{40}Ar/^{39}Ar$ thermochronology of Hbl, Kfs, Bt and Ms, which show cooling through 510 °C between 13 and 15 Ma and through 300–400 °C between 7 and 12 Ma (Boutonnet et al., 2012; Dunlap et al., 1998; Mukherjee et al., 2012).

The PMC (Fig. 1b) lies to the NE of the Pangong strand of the KFZ, extending from the NW shore of Pangong Tso to the Shyok River (Phillips, 2008), and consists of a sequence of interlayered amphibolites, marbles, psammites and Grt + St metapelitic schists (Fig. 2c–d). Grt + St metapelites were metamorphosed at peak sillimanite-grade conditions at c. 108 Ma (Streule et al., 2009) and then subsequently metamorphosed under staurolite-grade conditions of 585–605 °C, 605–725 MPa prior to initiation of the KFZ (Streule et al., 2009). Calcite grain size in PMC marbles records grain growth under temperatures of

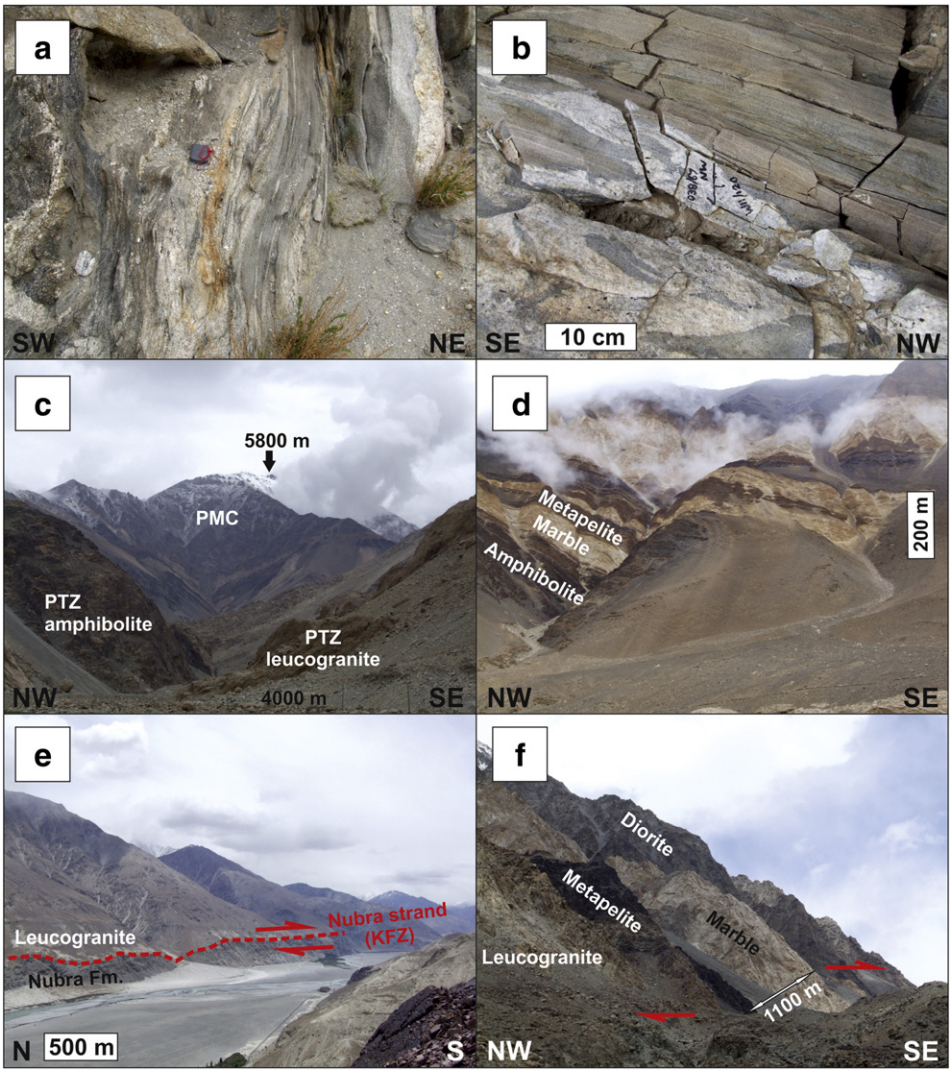

Fig. 2. Field photographs of the Eastern Karakoram Metamorphic Complex. (a) Diatexite migmatite in the PTZ near Muglib. Migmatite is partitioned into leucosome and melanosome (centre) and leucogranitic melt segregations (far right). Compass-clinometer (centre) is 8 cm. (b) Amphibolite (grey) intruded by irregular leucogranite dykes (white) in the PTZ near Taruk. (c) Gorge between Tangtse and Muglib. PTZ lithologies are juxtaposed with the PMC by the Pangong fault strand (out of shot at base of mountain). Foreground field of view is 450 m. (d) Layered sequence of PMC marble, amphibolite and metapelite near Pangong Tso. Field of view is 2.3 km. (e) The Nubra Formation juxtaposed with the Nubra–Siachen leucogranite by the Nubra fault strand of the KFZ in the Nubra Valley. (f) The Saser Formation in Sumur gorge. Metapelites and marbles within the Arganglas fault strand have accommodated dextral offset of the Nubra–Siachen leucogranite and Arganglas diorite.

300–480 °C, in accord with a temperature of c. 460 °C estimated from the mineralogy of an interlayered Bi + Pl schist (Rutter et al., 2007).

The Nubra Formation (Fig. 1b) extends between Yulskam and Rale as a KFZ-parallel band of metavolcanic and metapelitic rocks with subordinate marbles (Fig. 2e, Phillips, 2008). Nubra Formation metavolcanic rocks show peak metamorphism in the greenschist facies, characterised by the growth of epidote and chlorite in andesitic metavolcanic lithologies (Wallis et al., 2013). Metapelites have been metamorphosed to Grt + Ky grade but have undergone widespread synkinematic greenschist facies retrogression within the Nubra strand of the KFZ (Wallis et al., 2013).

The Saser Formation (Fig. 1b) crops out as a 35 km long band of Grt metapelites and marbles parallel to the Arganglas strand of the KFZ in the Saser Muztagh range (Fig. 2f, Phillips and Searle, 2007). No previous thermobarometry has been carried out on the Saser Formation.

KFZ deformation microstructures within the EKMC have previously been described in detail (Phillips and Searle, 2007; Rutter et al., 2007; Wallis et al., 2013). They include irregular lobate grain boundaries and subgrains in quartz and bulging grain boundaries and core–mantle structures in feldspar within metapelites. These features indicate deformation temperatures of c. 400–550 °C at strain rates of c. 10^{-13} s^{-1} (Wallis et al., 2013). Marbles contain twins and recrystallised grains typical of deformation under greenschist to sub-greenschist conditions (Rutter et al., 2007; Wallis et al., 2013). The metapelites of the Nubra Formation also contain a prominent band of greenschist facies phyllonite (Phillips and Searle, 2007; Wallis et al., 2013). The mineralogy and microstructure of the samples analysed in this study are described below in order to relate the deformation and metamorphic histories of the units.

3. Mineralogy and microstructure

The mineralogy and microstructures of seven samples, covering the four subunits of the EKMC (locations in Table 1), were analysed using standard optical microscopy and the FEI Quanta 650 FEG-ESEM at the University of Leeds.

W11/73 (Fig. 2a) is a melanocratic migmatite restite from the NE PTZ close to Muglib (Fig. 1b), with the assemblage Am + Pl + Bt + Qtz + Kfs (Fig. 3a). It has a fresh coarse (c. 0.5 mm) grained nematoblastic texture. Amphiboles show green-light brown pleochroism and lack intragranular deformation. Plagioclase shows occasional subgrains. Foliation is defined by aligned amphibole, biotite and elongate plagioclase.

W11/121 (Fig. 2b) is a fine grained nematoblastic amphibolite from the SW PTZ near Taruk (Fig. 1b) and consists of Pl + Qtz + Am + Ep + Ttn (Fig. 3b). Amphiboles are fragmented and anhedral with green-brown pleochroism. Plagioclase contains subgrains and quartz has irregular lobate grain boundaries.

P59 (Fig. 2c) is a fine grained nematoblastic amphibolite from the PMC near Muglib (Fig. 1b), consisting of Am + Pl + Qtz + Il (Fig. 3c). Amphiboles are brown in plane polarised light with subgrains visible in cross-polarised light. Plagioclase also contains subgrains and quartz has irregular lobate grain boundaries.

P121 (Fig. 2d) is a coarse grained amphibolite from the PMC near Pangong Tso (Fig. 1b), with the assemblage Am + Pl + Chl + Qtz + Cal + Rt (Fig. 3d). Alignment of c. 1 mm amphibole and c. 0.5 mm chlorite grains imparts a nematoblastic–lepidoblastic texture. Amphiboles show green-blue pleochroism, undulose extinction and

Table 1
Sample locations and representative chemical compositions of minerals used for geothermobarometry.

Sample	W11/73		W11/121		P59		P121		P85	P146
Lithology	Migmatite melanosome		Amphibolite		Amphibolite		Amphibolite		Meta-pelite	Meta-pelite
Lat.	34°02.738′		34°00.838′		34°04.512′		33°57.889′		34°42.644′	34°35.425′
Long.	078°13.452′		078°08.925′		077°35.274′		078°24.613′		077°35.274′	077°44.262′
Mineral	Am	Pl	Am	Pl	Am	Pl	Am	Pl	Bt	Bt
SiO_2	44.02	61.26	42.44	59.60	44.75	56.77	42.37	62.09	35.60	35.11
TiO_2	0.99	0.03	0.57	0.02	0.63	0.01	0.50	0.03	2.12	2.76
Al_2O_3	10.73	24.58	11.06	26.09	13.58	27.92	15.23	24.45	19.59	17.96
Cr_2O_3	0.08	na	0.04	na	0.12	na	0.10	na	0.12	0.01
Fe_2O_3	2.88	0.19	4.05	0.13	2.47	0.18	3.24	0.14	0.00	0.00
FeO	12.24	na	15.78	na	11.58	na	12.79	na	20.72	22.38
MnO	0.41	0.01	0.78	0.06	0.38	0.00	0.30	0.01	0.20	0.38
MgO	11.98	0.00	8.74	0.03	11.68	0.00	9.97	0.01	8.34	7.53
Cao	11.89	6.19	11.89	7.50	11.41	9.58	11.35	5.54	0.03	0.01
Na_2O	1.42	8.23	1.21	7.36	1.49	6.45	1.87	8.94	0.24	0.13
K_2O	1.29	0.29	1.33	0.12	0.27	0.05	0.28	0.07	8.63	9.43
H_2O	2.00	na	1.90	na	2.07	na	2.03	na	3.95	3.89
F	0.04	na	0.11	na	0.00	na	0.00	na	na	na
Cl	0.03	na	0.08	na	0.00	na	0.02	na	na	na
Ba	na	0.14	na	0.00	na	0.00	na	0.00	na	na
Sum	100.00	100.92	99.98	100.91	100.43	100.96	100.05	101.28	99.54	99.59
Oxygens	23	8	23	8	23	8	23	8	22	22
Si	6.522	2.706	6.442	2.637	6.488	2.528	6.241	2.725	5.406	5.418
Ti	0.110	0.001	0.065	0.000	0.069	0.000	0.055	0.001	0.242	0.320
Al	1.874	1.280	1.978	1.360	2.320	1.465	2.644	1.265	0.912	0.685
Cr	0.009	na	0.004	na	0.014	na	0.012	na	0.014	0.001
Fe_3	0.321	0.006	0.462	0.004	0.269	0.006	0.359	0.005	0.000	0.000
Fe_2	1.517	na	2.003	na	1.404	na	1.575	na	2.631	2.888
Mn	0.052	0.000	0.100	0.002	0.046	0.000	0.037	0.000	0.026	0.049
Mg	2.646	0.000	1.977	0.002	2.524	0.000	2.189	0.001	1.888	1.733
Ca	1.888	0.293	1.934	0.355	1.773	0.457	1.792	0.260	0.006	0.002
Na	0.408	0.705	0.356	0.631	0.419	0.557	0.534	0.760	0.070	0.040
K	0.244	0.016	0.257	0.007	0.049	0.003	0.052	0.004	1.672	1.858
Ba	na	0.002	na	0.000	na	0.000	na	0.00	na	na
Sum	15.591	5.009	15.578	4.998	15.375	5.016	15.490	5.021	12.867	12.994
XAn	–	28.79	–	36.23	–	46.03	–	27.07	–	–
XMg	–	–	–	–	–	–	–	–	0.42	0.38

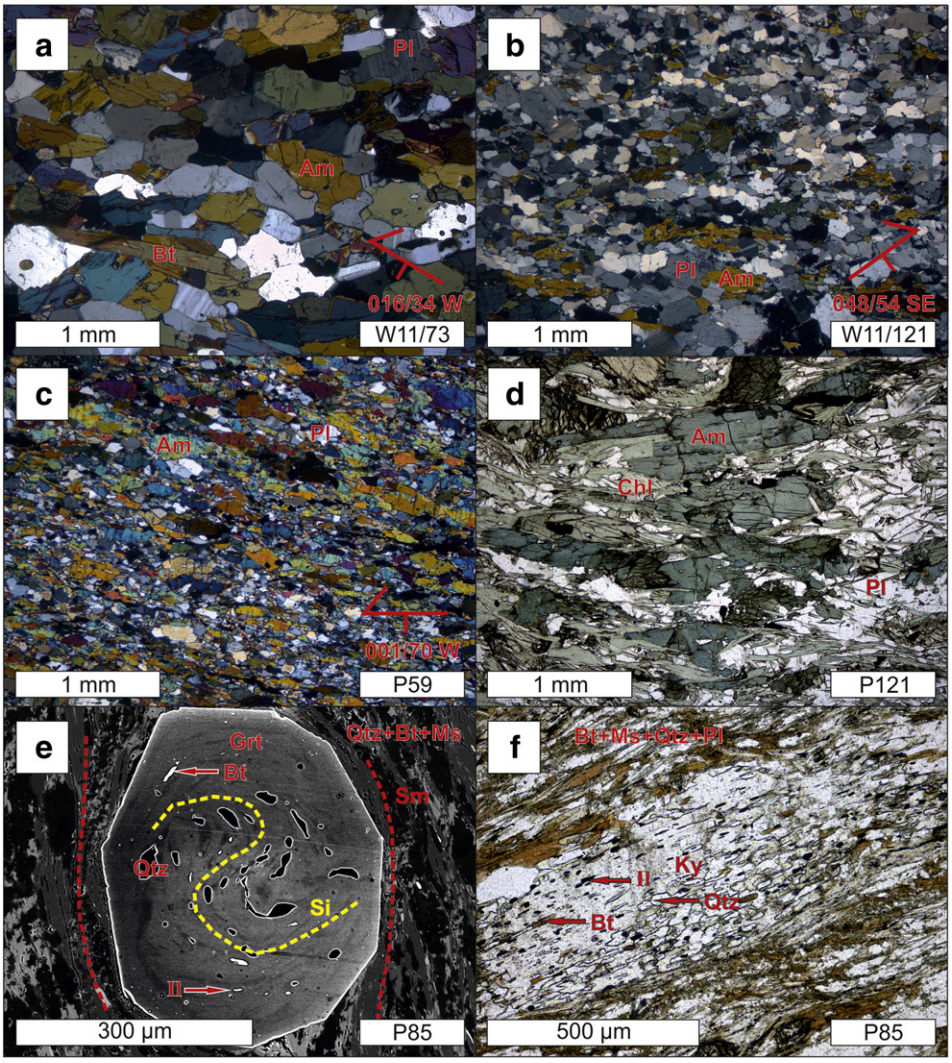

Fig. 3. Microstructures within the Eastern Karakoram Metamorphic Complex. (a)–(c) are cross-polarised optical photomicrographs. (d) and (f) are plane-polarised optical photomicrographs. (e) is a composite backscattered electron atomic number contrast image with brightness/contrast adjusted separately for garnet and matrix. (a) W11/73, PTZ, coarse grained migmatite restite with weak grain alignment fabric. (b) W11/121, PTZ, plagioclase-rich amphibolite with elongate amphiboles. (c) P59, PMC, amphibolite with strong amphibole grain alignment fabric. (d) P121, PMC, amphibolite with blue-green amphiboles in chloritic matrix. (e) P85, Nubra Formation metapelite. Sigmoidal zoning and Qtz + Bi + Il inclusion fabric (Si) is discordant with matrix foliation (Sm). (f) P85, Nubra Formation metapelite. Kyanite porphyroblast with Qtz + Bi + Il inclusions. Am = amphibole, Bt = biotite, Chl = chlorite, Grt = garnet, Il = ilmenite, Ky = kyanite, Ms = muscovite, Pl = plagioclase, Qtz = quartz.

are fractured. Plagioclase contains subgrains and has bulging grain boundaries.

P85 (Fig. 2e) is a fine grained metapelite from the Nubra Formation (Fig. 1b), consisting of Bt + Ms + Qtz + Pl + Grt + Ky + Il (Fig. 3e and f). It comprises a matrix of strongly lepidoblastic Bt + Ms + Qtz + Pl, which asymmetrically wraps around idioblastic garnet and nematoblastic kyanite porphyroblasts to define a dextral S–C fabric striking c. 140° parallel to the macroscopic trend of the KFZ. Garnet and kyanite porphyroblasts contain quartz, biotite and ilmenite inclusions. In kyanite these inclusions are aligned parallel to the long axis of kyanite blades (Fig. 3f). In garnet the inclusions define straight or sigmoidal fabrics, both of which are discordant to the matrix foliation (Fig. 3e). Quartz ribbons within the matrix contain abundant subgrains.

W11/30 (Fig. 2e) is a porphyroblastic metapelite from the Nubra Formation adjacent to the Nubra–Siachen leucogranite batholith (Fig. 1b), with the assemblage Bt + Qtz + And + Grt + Ms. Andalusite porphyroblasts up to 5 mm in length are aligned within a fine grained, well foliated Qtz + Bt + Ms matrix and contain quartz and biotite inclusions. The latter are of similar size to matrix biotite but show little or no preferred alignment (Fig. 4a–c). The quartz inclusions are very fine grained rods aligned sub-perpendicular to the long axis of andalusite blades. Andalusite grain boundaries are irregular and overgrown by a thin layer of muscovite that coarsens into pressure shadows (Fig. 4b). Coarse grained quartz also occurs in these pressure shadows (Fig. 4d–e), as well as in monomineralic layers. In these microstructures, quartz has irregular lobate grain boundaries, weak subgrain development but strong undulose extinction. Finer grained matrix quartz shows abundant subgrains. Small garnets occur within andalusite-free layers. A few contain fine graphite inclusions but most are optically inclusion free. The Bt + Ms foliation is oriented 138/80 NE, parallel to the macroscopic orientation of the KFZ and wraps around both andalusite (Fig. 4e) and garnet (Fig. 4f) porphyroblasts with dextral asymmetry. Andalusite growth only occurs within a few metres of the Nubra–Siachen leucogranite batholith. At greater distances, kyanite bearing assemblages (P85) are preserved.

P146 (Fig. 2f) is a K-feldspar megacrystic lepidoblastic metapelite from the Saser Formation (Fig. 1b), with the assemblage Pl + Kfs + Qtz + Bt + Ms + Il (Wallis et al., 2013). Alignment of micas and quartz ribbons form a strong dextral S–C fabric showing simple shear, consistent with the KFZ deformation in the Arganglas strand of the fault

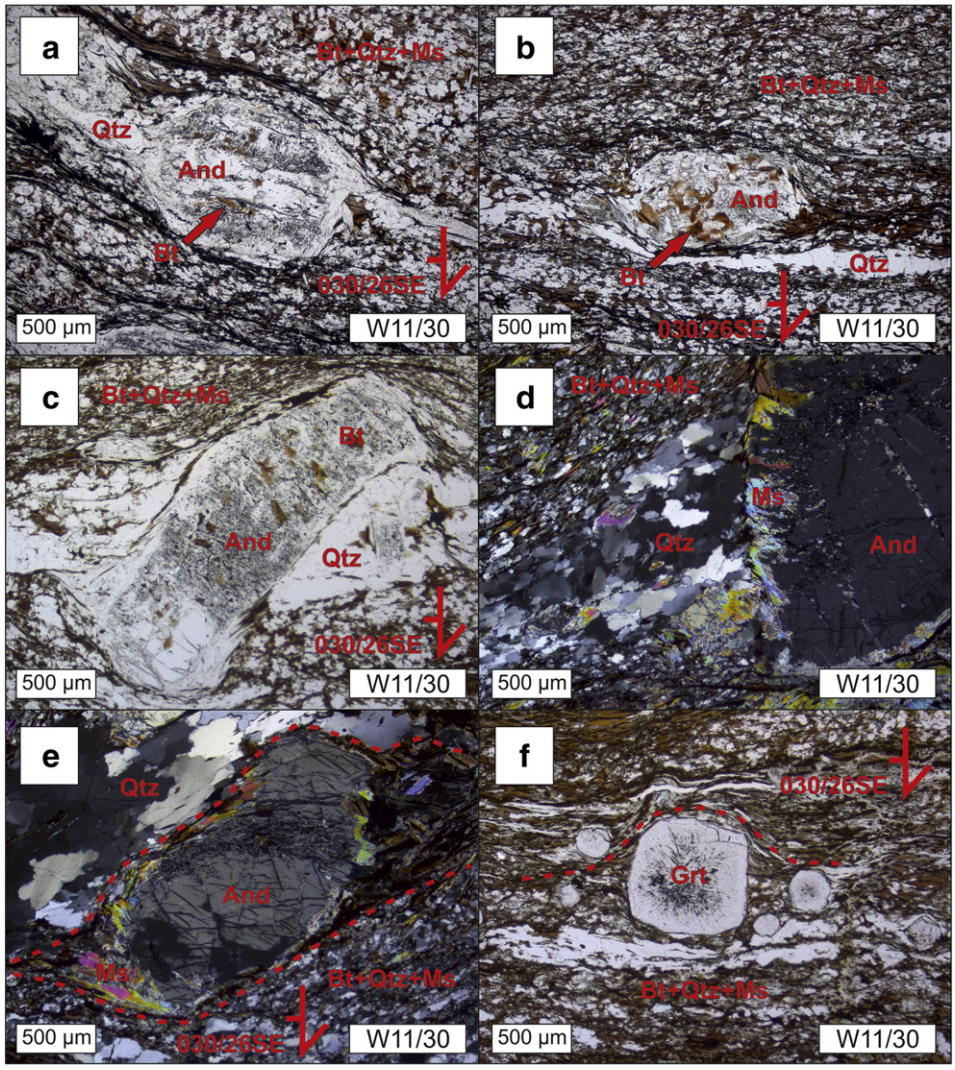

Fig. 4. Microstructures in W11/30 Nubra Formation metapelite. (a–c and f) are plane-polarised optical photomicrographs. (d) and (e) are cross-polarised optical photomicrographs. (a–c) Andalusite porphyroblasts with randomly oriented biotite inclusions and quartz pressure shadows (a and c), wrapped by Bt + Qtz + Ms matrix with dextral shear sense (c). (d) Andalusite porphyroblast with muscovite overgrowth and coarse quartz pressure shadow. (e) Andalusite porphyroblast with muscovite overgrowth and biotite pressure shadow showing dextral shear sense. (f) Foliation wrapping around garnet porphyroblast. Bt = biotite, Qtz = quartz, Ms = muscovite, And = andalusite and Grt = garnet.

(Phillips and Searle, 2007). The same dextral shear sense is also shown by σ-type mantled feldspar porphyroclasts and sigmoidal and rhomboidal muscovite fish. Ribbon quartz shows interlocking lobate grain boundaries, whereas feldspars show bulging grain boundaries and fine grained recrystallised mantles (Wallis et al., 2013).

4. Data collection and geothermobarometers

4.1. Amphibole–plagioclase thermobarometry

Amphibole and plagioclase major element data were collected using wavelength-dispersive X-ray spectroscopy on the Jeol 8230 electron microprobe at the University of Leeds. Amphibole analyses were collected using 15 kV accelerating voltage, 15 nA beam current and a <1 μm focussed beam. Peak and background count times were respectively 30 s and 15 s for Fe, 20 s and 10 s for Si and Al and 10 s and 5 s for remaining elements (see Table 1). Plagioclase analyses were collected using 15 kV accelerating voltage, 10 nA beam current and a 2 μm beam. Peak and background count times were respectively 30 s and 15 s for Fe and 10 s and 5 s for remaining elements (see Table 1). Measurements were made in pairs from the margins of adjacent amphibole and plagioclase grains. 35 amphibole–plagioclase pairs were analysed for W11/73, 32 for W11/121 and 15 pairs each for P59 and P121 (Supplement 1).

Pressure estimates were derived using the geobarometric calibrations of Anderson and Smith (1995) and Bhadra and Bhattacharya (2007) (Supplements 2 and 3). The geobarometer of Anderson and Smith (1995) is based on increasing Al-content of amphibole with pressure. It accounts for the effects of temperature and fO_2 and is valid in the range 100–1000 MPa and 675–760 °C. This barometer was experimentally calibrated using igneous melt-bearing assemblages and therefore is most appropriate to these rock types. The barometer of Bhadra and Bhattacharya (2007) is based on elemental distributions between equilibrated amphibole–plagioclase pairs and was calibrated against experimental quartz-bearing assemblages for the range 1–15 MPa and 650–950 °C, with the aim of developing a barometer applicable to garnet-free metamorphic rocks. Two calibrations of the Bhadra and Bhattacharya (2007) barometer were developed using different input parameters for regression. These two expressions yield similar results for our samples, differing by only 20 MPa on average, so we report the average of the two results. Due to the different calibration assemblages of the two barometers the Anderson and Smith (1995) barometer is most appropriate for rocks that equilibrated in the presence of melt (i.e. migmatite W11/73), whereas the Bhadra and Bhattacharya

(2007) barometer is most appropriate for amphibolites (i.e. W11/121, P59 and P121). We include however the results of both calibrations for all four of these samples for comparison.

Temperature estimates were made using the geothermometer calibrations of Holland and Blundy (1994) and Otten (1984). The Holland and Blundy (1994) calibration is based on the reaction edenite + albite = richterite + anorthite (Anderson, 1996) and was calibrated using both experimental data and natural igneous and metamorphic assemblages. The Otten (1984) thermometer uses an empirical calibration of the Ti-content of natural igneous amphiboles, but lacks the thermodynamic rigour of the Holland and Blundy (1994) geothermometer. As the Holland and Blundy (1994) thermometer was calibrated for both igneous and metamorphic assemblages and has a strong thermodynamic basis we favour these results over those of the Otten (1984) geothermometer. Nevertheless, the Otten (1984) temperature estimates are included for comparison with the Holland and Blundy (1994) amphibole–plagioclase estimates and the Henry et al. (2005) Ti-in-biotite geothermometer (Section 4.2). Pressures using the Anderson and Smith (1995) calibration and temperatures using the Holland and Blundy (1994) and Otten (1984) calibrations were determined using the "Plagioclase–Hornblende Thermobarometry" spreadsheet available from the Mineralogical Society of America at www.minsocam.org/MSA/RIM/RiM69_Ch04_hbld_plag_thermo-jla.xls (Supplement 3). Pressures from the Bhadra and Bhattacharya (2007) geobarometer were also used as input to this spreadsheet to determine the corresponding Holland and Blundy (1994) temperatures.

4.2. Ti-in-biotite geothermometry

Major element data were collected on biotites using the Jeol 8230 electron microprobe at the University of Leeds. Analysis conditions were 15 kV accelerating voltage and 15 nA beam current. Count times for peaks and backgrounds were respectively 60 s and 30 s for Ti and 15 s and 7 s for remaining elements (Table 1). Measurements were collected from biotite margins adjacent to ilmenite grains to ensure that the biotite is Ti-saturated. In total, 79 analyses were made on sample P85 and 41 on P146 (Supplement 4).

Temperature estimates were derived using the Ti-in-biotite geothermometer of Henry et al. (2005), which is based on the increase in Ti content of biotite with increasing temperature for given Mg/(Mg + Fe). This geothermometer is best applied to graphitic metapelites containing ilmenite/rutile, quartz and an aluminous phase (e.g. staurolite, cordierite or Al_2SiO_5), which respectively set Ti, Si and Al to maximum levels in the biotite. The calibration range of the geothermometer is 400–600 MPa pressure, Mg/(Mg + Fe) = 0.275–1.0 and Ti = 0.04–0.6 atoms per formula unit. Both P85 and P146 contain ilmenite and quartz and have Ti and Mg/(Mg + Fe) within the calibration range. Graphite is absent from the metapelites but the effect of this is currently poorly constrained. Éric et al. (2009) compared Ti-in-biotite temperature estimates for non-graphitic metapelitic assemblages against garnet–biotite, garnet–muscovite and THERMOCALC 3.21 temperature estimates. They found that the temperature estimates compared favourably in samples where Ti-content showed a negative correlation with Mg/(Mg + Fe) (a principle of the Ti-in-biotite method), but found discrepancies of up to 110 °C for samples where biotites showed a positive correlation. As biotites in both P85 and P146 show negative correlation between Ti-content and Mg/(Mg + Fe) (Supplement 4) the Ti-in-biotite temperatures may not be greatly affected by the absence of graphite. At present, the pressure of metamorphism is unconstrained. Pressures <400 MPa would result in an overestimation of temperature, whereas pressures over 600 MPa would result in underestimation of temperature. The P146 paragenesis lacks an Al-saturating phase so its Ti-in-biotite temperature may be an overestimate (Henry et al., 2005). As P85 only contains ilmenite as inclusions within garnet and kyanite, but not in its matrix, biotite in the matrix is likely to be Ti-undersaturated. Measurements were only taken therefore from biotite grains included within garnet and kyanite porphyroblasts. As a result, the Ti-in-biotite temperature for P85 records the temperature at the time of, or prior to, garnet and kyanite growth. The precision of the thermometer is estimated to be ±24 °C at <600 °C, improving to ±12 °C at >700 °C (Henry et al., 2005). Temperatures were determined using the "TiInBiotiteThermometer" spreadsheet available at http://www.geol.lsu.edu/henry/Research/biotite/TiInBiotiteGeothermometer.htm (Supplement 5) (Henry et al., 2005). We chose not to use garnet–biotite geothermometry as it is not clear in our garnet-bearing samples (P85, W11/30) whether the preserved garnet and biotite grew in equilibrium with one another.

5. Geothermobarometry results

5.1. Amphibole–plagioclase chemistry and P–T estimates

Representative amphibole and plagioclase compositional data are summarised in Table 1, whilst thermobarometry results are summarised in Table 2. The errors reported in the text account for both the calibration error and the spread of the measured values (two standard deviations) by taking the square root of the sum of both errors squared (Powell, 1978). This is also the case for the Ti-in-biotite results.

Amphiboles in W11/73 are dominantly edenite. They have low Al-contents of 1.51–1.96 atoms per 23 oxygens and mean Ca and Na of 1.89 and 0.39 respectively. Plagioclases are dominantly oligoclase with An in the range 27.3–31.6 with a mean value of 28.8. These compositions give a relatively small spread of amphibole–plagioclase temperature and pressure estimates with mean values of 688 ± 44 °C and 522 ± 91 MPa respectively. Ti-contents of amphibole (mean 0.10 atoms per 23 O) give a temperature of 667 ± 35 °C, within error of the amphibole–plagioclase temperature.

Amphiboles in W11/121 are dominantly potassic-hastingsite or magnesiohornblende. They have high Ca-content of 1.90–1.95 atoms per 23 oxygens. Mean Al-content is 1.91 atoms per 23 O. Plagioclases are dominantly andesine with An in the range 28.1–41.6 and a mean value of 36.2. These compositions give amphibole–plagioclase temperature and pressure estimates of 728 ± 56 °C and 875 ± 227 MPa. Mean amphibole Ti-contents of 0.06 atoms per 23 O give a temperature of 620 ± 39 °C, significantly lower than the amphibole–plagioclase temperature.

Amphiboles in P59 are magnesiohornblende and tschermakite. They have high Al-content of 2.06–2.39 atoms per 23 oxygens and mean Ca and Na of 1.78 and 0.41 respectively. Plagioclases are andesine with An in the range 37.3–50.3 and a mean value of 44.3. These compositions give amphibole–plagioclase temperature and pressure estimates of 736 ± 47 °C and 1059 ± 219 MPa. Mean amphibole Ti-contents of 0.08 atoms per 23 O give a temperature of 634 ± 27 °C, c. 100 °C lower than the amphibole–plagioclase temperature.

Amphiboles in P121 are predominantly tschermakite with some magnesiohornblende, pargasite and alumino pargasite. They have the highest Al-contents of 1.92–2.95 atoms per 23 O. They also have the lowest Ca and highest Na with mean values of 1.77 and 0.53 atoms per 23 oxygens respectively. Plagioclases are dominantly oligoclase with An in the range 22.9–36.0 and a mean value of 26.3. These compositions give temperature and pressure estimates of 677 ± 51 °C and 893 ± 215 MPa. Mean amphibole Ti-contents of 0.04 atoms per 23 O give a temperature of 597 ± 35 °C, again significantly lower than the amphibole–plagioclase temperature.

5.2. Biotite chemistry and temperature estimates

Representative biotite compositional data are given in Table 1, whilst Ti-in-biotite thermometry results are summarised in Table 2.

Biotites in P85 range in composition, with Mg/Mg + Fe of 0.36–0.45 (mean 0.42) and Ti-contents ranging between 1.24 and 2.89 wt.% or 0.14–0.34 atoms per 22 oxygens (mean 0.24). These compositions

Table 2
Amphibole–plagioclase thermobarometry and Ti-in-biotite thermometry results and estimated geothermal gradients.[a]
AS95 and BB07 are the barometer calibrations of Anderson and Smith (1995) and Bhadra and Bhattacharya (2007) respectively. HB94, O84 and H05 are the thermometer calibrations of Holland and Blundy (1994), Otten (1984) and Henry et al. (2005) respectively.

Amphibole–plagioclase thermobarometry

Sample	Geobarometer and calibration error	Pressure (MPa) (±2σ)	Temperature (°C)		Geothermal gradient (°C/km)	
			HB94 (±40 °C) (±2σ)	O84 (±25 °C) (±2σ)	T from HB94	T from O84
W11/73	**AS95 (±60 MPa)**	**522 ± 68**	**688 ± 18**	667 ± 24	**36 ± 7**	35 ± 6
	BB07 (±200 MPa)	439 ± 67	684 ± 18		43 ± 21	42 ± 20
W11/121	AS95 (±60 MPa)	550 ± 100	711 ± 40	620 ± 30	36 ± 8	31 ± 7
	BB07 (±200 MPa)	**875 ± 108**	**728 ± 39**		**23 ± 6**	19 ± 5
P59	AS95 (±60 MPa)	720 ± 64	699 ± 24	634 ± 11	28 ± 4	24 ± 3
	BB07 (±200 MPa)	**1059 ± 90**	**736 ± 24**		**19 ± 4**	16 ± 3
P121	AS95 (±60 MPa)	898 ± 254	679 ± 44	597 ± 25	21 ± 6	18 ± 5
	BB07 (±200 MPa)	**893 ± 80**	**677 ± 32**		**21 ± 5**	18 ± 5

Ti-in-biotite thermometry

Sample	Geothermometer and calibration error	Temperature (°C) (±2σ)
P85	**H05 (±20 °C)**	**622 ± 36**
P146	**H05 (±20 °C)**	**656 ± 36**

[a] Most appropriate geothermometer–barometer combinations for each sample are highlighted in bold (see main text). Calibration errors are given with the calibrations. P–T results are given with two standard deviations of the spread of results within each sample. Errors on the geothermal gradient estimates were propagated from the quadratically combined calibration and result errors.

give a temperature estimate of 605 ± 45 °C. Of the 79 temperature estimates, 78.5% are closely grouped within the top portion of the range (592–669 °C) (Supplement 5). The remaining 21.5% of the estimates drop off rapidly to temperatures as low as 479 °C, suggesting that these measurements were made on biotites equilibrated with the Ti-undersaturated matrix. This may result from the grains not being fully encased by host garnet or kyanite in directions out of section. If these anomalously low temperatures (<592 °C) are excluded, a more refined estimate of 622 ± 41 °C is obtained.

Biotites in P146 have a more limited range of compositions, with Mg/(Mg + Fe) of 0.35–0.40 (mean 0.38) and Ti-contents ranging between 1.91 and 3.40 wt.% or 0.22–0.39 atoms per 22 oxygens (mean 0.32). These compositions give a temperature estimate of 656 ± 41 °C.

6. Metamorphism and deformation of the Eastern Karakoram Metamorphic Complex

6.1. The Pangong Transpressional Zone

Phillips et al. (2013) determined a U–Pb age of 17.4 ± 0.4 Ma for a migmatite leucosome from the PTZ near Muglib. Amphibole–plagioclase thermobarometry of sample W11/73 provides the conditions of equilibration for a migmatite melanosome from the same unit. The results of 688 ± 44 °C, 522 ± 91 MPa (sillimanite stability field) are considered therefore to be the conditions under which anatexis occurred at c. 17–18 Ma (Fig. 5). The temperature estimate is similar to the 675–750 °C melting temperature suggested by Reichardt et al. (2010) and the pressure estimate is within error of 570 ± 20 MPa determined for the migmatite unit by Reichardt and Weinberg (2012). These results also fall slightly above the "wet" granite solidus (Wyllie, 1977). Alignment of amphibole, biotite and elongate plagioclase indicate that migmatisation occurred under deviatoric stress. Rare plagioclase subgrains suggest limited deformation at near solidus conditions (>600 °C) (Tullis and Yund, 1985). This sample lacks evidence of lower temperature deformation (e.g. bulging grain boundaries in feldspar).

Sample W11/121 from the opposite side of the PTZ near Taruk (Fig. 5) yields significantly higher estimates (728 ± 56 °C, 875 ± 227 MPa, kyanite–sillimanite boundary) than W11/73, indicating that these samples record distinct portions of the unit's pressure–temperature–time path. The pressure estimate for W11/121 is within error of those for samples P59 and P121 in the PMC. Subgrains in plagioclase and lobate grain boundaries in quartz indicate deformation by subgrain rotation and grain boundary migration dynamic recrystallization respectively, suggesting deformation temperatures of >600 °C (Stipp et al., 2002; Tullis and Yund, 1985). The finer grain size and disaggregated amphibole suggest that W11/121 experienced higher stress and higher strain than W11/73.

The amphibole–plagioclase thermobarometry results can be used to estimate an apparent geothermal gradient at the time of metamorphic equilibration (e.g. Palin et al., 2012; Weller et al., 2013) by assuming a crustal density of 2.8 g/cm^3 and converting the pressure estimate to a depth estimate. As the true geothermal gradient was unlikely to be linear, such estimates provide only an approximate depth-averaged value. Nonetheless, this approach provides a relative means to compare thermal regimes. The thermobarometry results of W11/73 and W11/121 give geothermal gradients of 36 ± 7 °C/km and 23 ± 6 °C/km respectively (Fig. 5). The difference between these values suggests that the two samples equilibrated under different thermal regimes and record the evolving thermal state of this portion of the orogen. By the same assumptions, the results of Rolland and Pêcher (2001) and Rolland et al. (2009) give geotherms of >40 °C/km, 38–52 °C/km and 24–37 °C/km respectively for granulite, amphibolite and greenschist facies metamorphism within the PTZ. The result of 36 ± 7 °C/km for W11/73 suggests that the high geotherms predicted by Rolland and Pêcher (2001) and Rolland et al. (2009) may be somewhat overestimated.

Thanh et al. (2011) report conditions of 680 °C and 850 MPa for a Grt + Ky + St gneiss (sample 202A) within the PTZ, defining an apparent geothermal gradient of 22 °C/km. Although the age of this metamorphism is unconstrained, Thanh et al. (2011) attribute it to crustal thickening following the India–Asia collision. The pressure recorded by this sample is significantly greater than that of migmatite W11/73 but remarkably similar to that of W11/121 and also P121 from the PMC. We suggest therefore that the pressure and temperature of the Grt + Ky + St gneiss may record metamorphism broadly coincident with that of W11/121 and the PMC samples.

6.2. The Pangong Metamorphic Complex

Sample P59 (736 ± 47 °C, 1059 ± 219 MPa) from the PMC records high pressure (c. 38 km burial) within the kyanite stability field. These results define a low apparent geothermal gradient of 19 ± 4 °C/km, within error of those for the three other PMC and PTZ kyanite-grade samples (P121, W11/121 and 202A), but significantly lower than W11/73 in the PTZ. Amphibole and plagioclase subgrains suggest

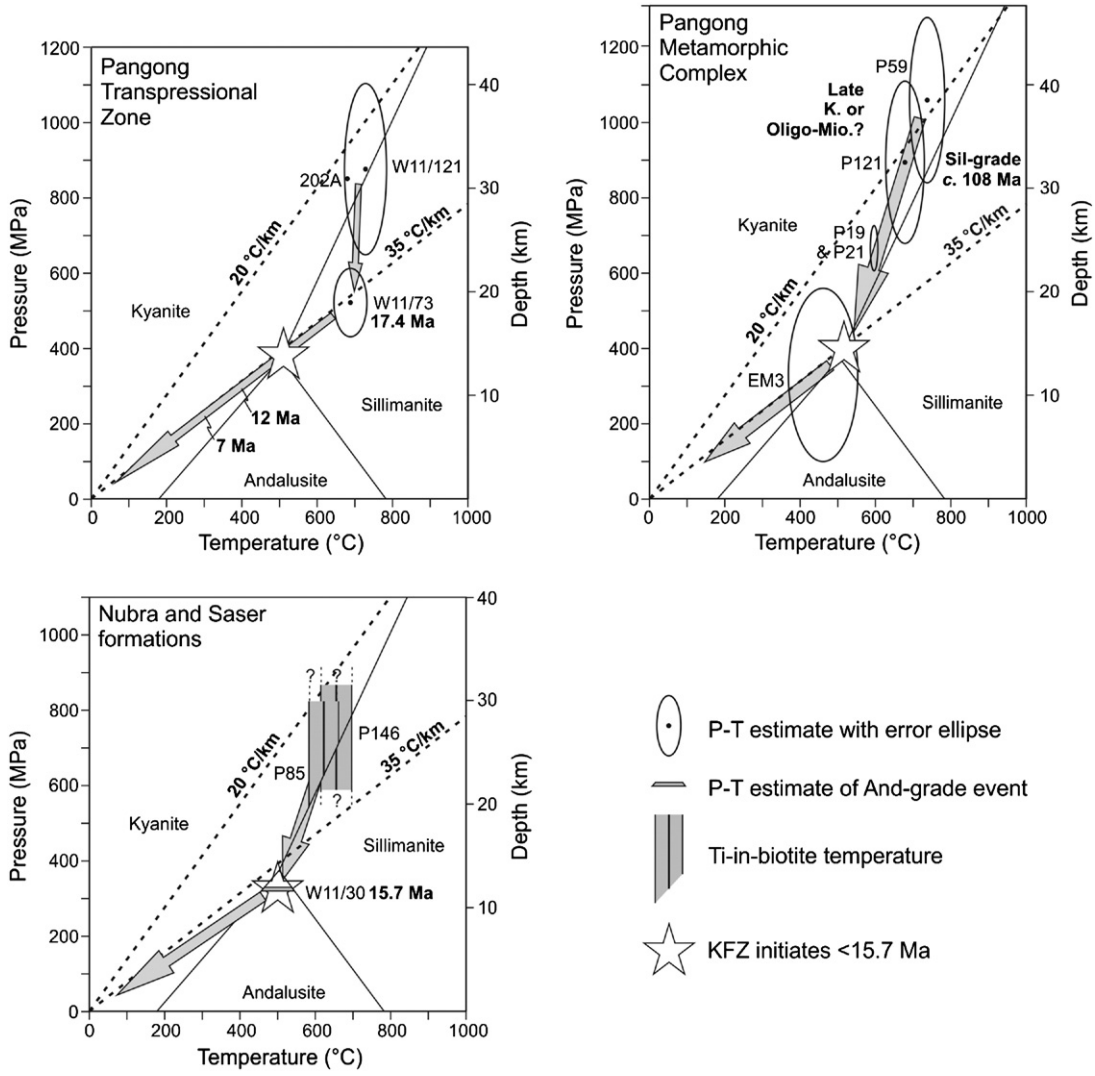

Fig. 5. Pressure–temperature–time paths of the Eastern Karakoram Metamorphic Complex.
Data compiled from this study, Boutonnet et al. (2012), Phillips et al. (2004, 2013), Reichardt and Weinberg (2012), Rutter et al. (2007), Streule et al. (2009) and Thanh et al. (2011). Also shown are geothermal gradients (dashed black lines) and Al_2O_5 polymorph stability fields after Holdaway (1971) and Holdaway and Mukhopadhyay (1993).

deformation at >650 °C (Kruse and Stünitz, 1999; Tullis and Yund, 1985), resulting in a similar microstructure to W11/121.

Sample P121 (677 ± 51 °C, 893 ± 215 MPa, kyanite stability field close to the sillimanite boundary) defines a low apparent geothermal gradient of 21 ± 5 °C/km (Fig. 5). Its proximity to the Bangong–Nujiang suture, the low apparent geothermal gradient and the presence of Na-rich blue-green amphibole (e.g. Fryer et al., 1999) provide evidence to suggest that metamorphism of P121 may have occurred within a forearc setting prior to, or around the time of, collision of the Ladakh island arc terrane with the Karakoram continental arc. This collision event and associated metamorphism of the Karakoram terrane occurred during the Late Cretaceous (Palin et al., 2012) and therefore would define the minimum age at which metamorphism of P121 occurred. Late Cretaceous sillimanite-grade metamorphism at 108 ± 0.6 Ma is recorded by sillimanite inclusions in garnet within the PMC metapelites and has been interpreted to result from Andean-type tectonism along the south Asian margin (Streule et al., 2009). Metamorphism of P121 therefore could have occurred at a similar time, corresponding to the M_0 event in the Hunza and Baltoro regions.

An alternative hypothesis is that kyanite-grade metamorphism in the PMC and PTZ correlates with the M_2 kyanite-grade metamorphism in the Baltoro and Hunza regions, which occurred during the Oligo-Miocene (Fraser et al., 2001; Palin et al., 2012; Searle et al., 2010). Retrograde staurolite-grade metamorphism of the PMC (585–605 °C 605–725 MPa, Fig. 5) is constrained to have occurred after Late Cretaceous sillimanite-grade metamorphism but before the initiation of the KFZ (Streule et al., 2009). If the widespread kyanite-grade metamorphism of the EKMC correlates with Oligo-Miocene kyanite-grade M_2 in the central Karakoram then the two regions could have shared the same metamorphic history of Cretaceous sillimanite-grade M_1, Oligo-Miocene kyanite-grade M_2 and Miocene staurolite-grade M_3 events (Palin et al., 2012). A comprehensive geochronological dataset aimed at constraining the timing of peak metamorphism across the EKMC is clearly required to distinguish between these correlations but is beyond the scope of the present study.

Plagioclase in P121 contains subgrains, indicating deformation at >600 °C, whilst bulging grain boundaries demonstrate that lower temperature deformation also occurred at 450–600 °C (Tullis and Yund, 1985). Further greenschist retrograde metamorphism is evidenced by chlorite overgrowths on amphibole in P121. Greenschist facies metamorphism of a Bt + Pl schist in the PMC occurred at 460 ± 92 °C and 330 ± 230 MPa (Fig. 5) and was synkinematic with respect to the KFZ (Rutter et al., 2007).

6.3. The Nubra Formation

Metapelite P85 records a Ti-in-biotite temperature of 622 ± 41 °C for biotite inclusions in garnet and kyanite. The stability of kyanite at 622 °C implies pressures greater than c. 650 MPa (Fig. 5). Sigmoidal zoning and aligned inclusions in garnet are discordant with the matrix foliation resulting from KFZ deformation. Thus, garnet growth and mid-amphibolite facies metamorphism of the Nubra Formation likely predate initiation of the KFZ. It is possible that garnet growth could have occurred during KFZ deformation and that discordant inclusion–matrix fabric relationships result from garnet rotation following the end of garnet growth. The randomly oriented and discordant inclusion fabrics in andalusite in the same sample however militate against this interpretation. Kyanite-grade metamorphism of the Nubra Formation, as with the PMC and PTZ, potentially correlates with the Oligocene–Miocene M_2 event in the central Karakoram, which is characterised by kyanite growth in both the Hunza and Baltoro regions (Fraser et al., 2001; Palin et al., 2012; Searle et al., 2010). Thus, the KFZ cut through the region following the end of the M_2 event at <21.8 Ma (Palin et al., 2012).

As andalusite growth (W11/30) occurs only within a few metres of the Nubra–Siachen leucogranite batholith, it most likely results from contact metamorphism during leucogranite emplacement at c. 15.87 ± 0.08 Ma (Phillips et al., 2004). Al-in-hornblende geobarometry indicates that the Nubra–Siachen leucogranite was emplaced at 320–330 MPa (Reichardt and Weinberg, 2012). Similar pressures are likely to have been experienced by the adjacent Nubra Formation during contact metamorphism (Fig. 5). Such pressures are close to the andalusite–sillimanite–kyanite triple point and therefore suggest temperatures of c. 500 °C in the wall rock metapelites. This temperature is consistent with estimates from deformation microstructures, such as quartz subgrains and lobate grain boundaries and bulging feldspar grain boundaries, formed within the KFZ shortly after leucogranite emplacement (samples P85, W11/30, P146; Phillips and Searle, 2007; Wallis et al., 2013). Randomly oriented biotite inclusions within andalusite grains wrapped by foliation formed during dextral simple shear (Fig. 4a–c) provide strong evidence to suggest that that the KFZ initiated after leucogranite emplacement (Phillips and Searle, 2007; Phillips et al., 2004). Andalusite is found also in the Baltoro batholith aureole in Pakistan (Searle et al., 2010), which constitutes the north-western continuation of the Nubra–Siachen leucogranite batholith (Phillips et al., 2004, 2013). This demonstrates the similar emplacement conditions of the two portions of the batholith. Subgrains and lobate grain boundaries in matrix and pressure shadow quartz (Fig. 4b and c) indicate that KFZ deformation occurred at 400–550 °C assuming strain rates of c. 10^{-12} s^{-1} (Stipp et al., 2002).

6.4. The Saser Formation

Metapelite sample P146 from the Saser Formation records a Ti-in-biotite temperature of 656 ± 41 °C (Fig. 5). P146 lacks an aluminous phase so this temperature is likely to be an overestimate as Al-undersaturation may cause changes in Ti substitution mechanism, resulting in elevated Ti levels in biotite (Henry and Guidotti, 2002; Henry et al., 2005). The true temperature of metamorphism may correlate therefore with either the slightly lower temperatures of 622 °C in the Nubra Formation or 585–605 °C for staurolite-grade metamorphism of the PMC (Streule et al., 2009). This result is the first estimate of metamorphic temperature for the Saser Formation and demonstrates that amphibolite grade metamorphism occurred across the EKMC.

7. Crustal evolution of the eastern Karakoram: relationship between metamorphism and strike-slip faulting

Mid-high temperature metamorphism of the EKMC in Ladakh resulted from a range of tectonic processes spanning the Early Cretaceous to Miocene. At c. 108 Ma, the eastern Karakoram formed an Andean-type margin (Phillips et al., 2013; Streule et al., 2009), resulting in sillimanite-grade metamorphism. Kyanite-grade metamorphism on low geothermal gradients (c. 19–23 °C/km) occurred either in a similar setting, before or after closure of the Shyok–Bangong–Nujiang suture (M_0 or M_1 respectively, Palin et al., 2012), or during post-India–Asia collision crustal thickening (M_2). In either case, metamorphism at 677–736 °C was pre- or syn-kinematic to similarly high temperature (>600 °C) regional deformation across the EKMC, corresponding to D0–D2 in the central Karakoram which occurred during regional crustal thickening (Phillips et al., 2013). In the PMC, this was followed by retrograde staurolite-grade metamorphism (Streule et al., 2009) and greenschist facies metamorphism, grain growth and deformation in marbles (Rutter et al., 2007). In the PTZ, additional tectonic uplift within the KFZ has exhumed a slice of Miocene migmatites from 19 to 20 km depth, which record an elevated geotherm (36 ± 7 °C/km), and juxtaposed them against older, more slowly exhumed, amphibolites. Pre-kinematic andalusite porphyroblasts in the Nubra Formation (Fig. 4a–c) indicate that the KFZ post-dates emplacement of the Nubra–Siachen leucogranite and are inconsistent with a syn-kinematic interpretation of magmatic structures in similar aged granitoids near Tangtse (Boutonnet et al., 2012; Leloup et al., 2011). As these microstructures, along with those in the leucogranites (Phillips and Searle, 2007; Phillips et al., 2004), indicate that the KFZ was not active in this region before c. 15.7 Ma, the 17.4 Ma migmatisation in the PTZ cannot be the result of shear heating (Fig. 5) and the KFZ cannot have acted to channel leucogranite magmas in the mid-crust (Lacassin et al., 2004b; Leech, 2008, 2009; Rolland and Pêcher, 2001; Rolland et al., 2009). These interpretations are consistent with the most recent findings along the southern portion of the KFZ, where it has been demonstrated to have initiated at c. 12 Ma (Wang et al., 2012, 2013a,b), rather than as early as up to 34 Ma (Lacassin et al., 2004a,b; Leloup et al., 2013; Valli et al., 2008). The findings of this study therefore support the interpretation that the KFZ propagated outwards from its north-central portion (Robinson, 2009; Wang et al., 2011, 2013a). High geothermal gradients during the Miocene, which resulted in upper amphibolite grade anatexis, were the result of crustal thickening and radiogenic heating, possibly exacerbated by mantle-derived magma heat input, in the broadly deforming crust across the Karakoram terrane (Searle et al., 2010, 2011). Kyanite-grade metamorphism of the Nubra Formation was overprinted by an andalusite-grade event during leucogranite emplacement. Later retrograde metamorphism and metasomatism of the EKMC occurred during exhumation and deformation within the KFZ (Wallis et al., 2013).

The record of Cretaceous subduction and Cenozoic crustal thickening, heating and anatexis preserved in the EKMC is equivalent to events recorded in the Baltoro and Hunza Karakoram to the northwest (Palin et al., 2012; Searle, 2013) and demonstrates the along-strike continuity of these processes. Pullen et al. (2011) discuss the similarities between the Qiantang mélange in Tibet and the geology of the Pamir in the northern Karakoram terrane. Whilst the eastern Karakoram has undergone a similar evolution to the southern Karakoram terrane in the Baltoro and Hunza regions, it does not reflect the antiformal structure of the Pamir and Qiangtang mélange (Pullen et al., 2011). Nor does it contain evidence of blueschist and eclogite facies metamorphism present within the Qiangtang mélange (Kapp et al., 2003; Pullen et al., 2011; Zhang et al., 2006). Correlation of the eastern Karakoram with the southern Karakoram, and the Qiangtang mélange with the northern Karakoram/Pamir supports low offsets of <150 km across the KFZ, as previously proposed due to the offset of several other geological markers (e.g. Murphy et al., 2000; Phillips et al., 2004; Robinson, 2009; Searle et al., 1998; Wang et al., 2012). Such correlation does not support the proposed larger offsets of several hundred kilometres (Lacassin et al., 2004a; Peltzer and Tapponnier, 1988; Valli et al., 2008).

8. Conclusions

Each sub-unit of the Eastern Karakoram Metamorphic Complex in Ladakh has undergone mid-upper amphibolite grade peak metamorphism with varying degrees of retrogression. Early Cretaceous subduction and crustal thickening along the southern Karakoram terrane resulted in sillimanite-grade metamorphism of the Pangong Metamorphic Complex. Kyanite-grade metamorphism under low geothermal gradients of 19–23 °C/km may have occurred at a similar time or possible later during the Oligo-Miocene. Additional geochronological studies are required to constrain the timing of this event. Subsequent upper amphibolite grade migmatisation in the Pangong Transpressional Zone occurred at c. 17.4 Ma under a higher geothermal gradient of 36 ± 7 °C/km. Microstructures in the Nubra Formation demonstrate that the Karakoram Fault Zone initiated after leucogranite emplacement at c. 15.7 Ma and after peak metamorphism. Thus the high geothermal gradients and anatexis recorded in the PTZ are not the result of shear heating but of regional crustal thickening and heating processes. The close similarity between metamorphism of the EKMC and that of the Karakoram metamorphic complex in Baltoro–Hunza supports limited offset on the KFZ of <150 km.

Supplementary data to this article can be found online at http://dx.doi.org/10.1016/j.tecto.2014.03.023.

Acknowledgements

We are grateful to Fida Hussain Mitoo of the New Royal Guest House, Leh, for logistical support in Ladakh. Andrew Parsons is thanked for assistance during fieldwork. We are grateful also to Eric Condliffe and Richard Walshaw for assistance with the electron microscope and microprobe. We thank an anonymous reviewer for their comments that helped to improve this paper. DW gratefully acknowledges support from NERC (training grant NE/I528750/1).

References

Anderson, J.L., 1996. Status of thermobarometry in granitic batholiths. Trans. R. Soc. Edinburgh 87, 125–138.
Anderson, J.L., Smith, D.R., 1995. The effect of temperature and oxygen fugacity on Al-in-hornblende barometry. Am. Mineral. 80, 549–559.
Bhadra, S., Bhattacharya, A., 2007. The barometer tremolite + tschmakite + 2 albite = 2 pargasite + 8 quartz: constraints from experimental data at unit silica activity, with application to garnet-free natural assemblages. Am. Mineral. 92, 491–502.
Boutonnet, E., Leloup, P.H., Arnaud, N., Paquette, J.-L., Davis, W.J., Hattori, K., 2012. Synkinematic magmatism, heterogeneous deformation, and progressive strain localization in a strike-slip shear zone: the case of the right-lateral Karakorum fault. Tectonics 31, TC4012.
Dunlap, W.J., Weinberg, R.F., Searle, M.P., 1998. Karakoram fault zone rocks cool in two phases. J. Geol. Soc. Lond. 155, 903–912.
Éric, S., Logar, M., Milovanović, D., Babič, D., Adnađević, B., 2009. Ti-in-biotite geothermometry in non-graphitic, peraluminous metapelites from Crni vrh and Resavski humovi (Central Serbia). Geol. Carpath. 60, 3–14.
Foster, G., Parrish, R.R., Horstwood, M.S.A., Chenery, S., Pyle, J., Gibson, H.D., 2004. The generation of prograde *P–T–t* points and paths; a textural, compositional and chronological study of metamorphic monazite. Earth Planet. Sci. Lett. 228, 125–142.
Fraser, J.E., Searle, M.P., Parrish, R.R., Noble, S.R., 2001. Chronology of deformation, metamorphism and magmatism in the southern Karakoram mountains. Geol. Soc. Am. Bull. 113, 1443–1455.
Fryer, P., Wheat, C.G., Mottl, M.J., 1999. Mariana blueschist mud volcanism: implications for conditions within the subduction zone. Geology 27, 103–106.
Henry, D.J., Guidotti, C.V., 2002. Titanium in biotite from metapelitic rocks: temperature effects, crystal-chemical controls, and petrologic applications. Am. Mineral. 87, 375–382.
Henry, D.J., Guidotti, C.V., Thomson, J.A., 2005. The Ti-saturation surface for low-to-medium pressure metapelitic biotite: implications for geothermometry and Ti-substitution mechanisms. Am. Mineral. 90, 316–328.
Holdaway, M.J., 1971. Stability of andalusite and aluminium silicate phase diagram. Am. J. Sci. 271, 97–131.
Holdaway, M.J., Mukhopadhyay, B., 1993. A re-evaluation of the stability relations of andalusite; thermochemical data and phase diagram for the aluminum silicates. Am. Mineral. 78, 298–315.
Holland, T., Blundy, J., 1994. Non-ideal interactions in calcic amphiboles and their bearing on amphibole–plagioclase thermometry. Contrib. Mineral. Petrol. 116, 433–447.
Kapp, P., Yin, A., Manning, C.E., Harrison, T.M., Taylor, M.H., Ding, L., 2003. Tectonic evolution of the early Mesozoic blueschist-bearing Qiangtang metamorphic belt, central Tibet. Tectonics 22, 1043.
Klemperer, S.L., Kennedy, B.M., Sastry, S.R., Makovsky, Y., Harinarayana, T., Leech, M.L., 2013. Mantle fluids in the Karakoram fault: helium isotope evidence. Earth Planet. Sci. Lett. 366, 59–70.
Kruse, R., Stünitz, H., 1999. Deformation mechanisms and phase distribution in mafic high-temperature mylonites from the Jotun Nappe, southern Norway. Tectonophysics 303, 223–249.
Lacassin, R., Valli, F., Arnaud, N., LeLoup, P.H., Paquette, J.L., Haibing, L., Tapponnier, P., Chevalier, M.-L., Guillot, S., Maheo, G., Zhiqin, X., 2004a. Large-scale geometry, offset and kinematic evolution of the Karakorum fault, Tibet. Earth Planet. Sci. Lett. 219, 255–269.
Lacassin, R., Valli, F., Arnaud, N., LeLoup, P.H., Paquette, J.L., Haibing, L., Tapponnier, P., Chevalier, M.-L., Guillot, S., Maheo, G., Zhiqin, X., 2004b. Reply to Comment on "Large-scale geometry, offset and kinematic evolution of the Karakorum fault, Tibet". Earth Planet. Sci. Lett. 229, 159–163.
Leech, M.L., 2008. Does the Karakoram fault interrupt mid-crustal channel flow in the western Himalaya? Earth Planet. Sci. Lett. 276, 314–322.
Leech, M.L., 2009. Reply to comment by M.P. Searle and R.J. Phillips (2009) and R.R. Parrish (2009) on: "Does the Karakoram fault interrupt mid-crustal channel flow in the western Himalaya?" by Mary L. Leech, Earth and Planetary Science Letters 276 (2008) 314–322. Earth Planet. Sci. Lett. 286, 592–595.
Leloup, P.H., Boutonnet, E., William, J.D., Hattori, K., 2011. Long-lasting intracontinental strike-slip faulting: new evidence from the Karakorum shear zone in the Himalayas. Terra Nova 23, 92–99.
Leloup, P.H., Boutonnet, E., Weinberg, R.F., Mukherjee, B.K., Tapponnier, P., Lacassin, R., Chevalier, M.L., Li, H., Valli, F., Arnaud, N., Paquette, J.L., 2013. Comment on "Displacement along the Karakoram fault, NW Himalaya, estimated from LA-ICP-MS U–Pb dating of offset geologic markers" published by Shifeng Wang et al. in EPSL, 2012. Earth Planet. Sci. Lett. 363, 242–245.
Mukherjee, B.K., Sen, K., Sachan, H.K., Paul, S.K., 2012. Exhumation history of the Karakoram fault zone mylonites: new constraints from microstructures, fluid inclusions, and ^{40}Ar–^{39}Ar analyses. Lithosphere 4, 230–241.
Murphy, M.A., Yin, A., Kapp, P., Harrison, T.M., Lin, D., Jinghui, G., 2000. Southward propagation of the Karakoram fault system, southwest Tibet: timing and magnitude of slip. Geology 28, 451–454.
Otten, M.T., 1984. The origin of brown amphibole in the Artfjället gabbro and dolerites. Contrib. Mineral. Petrol. 86, 189–199.
Palin, R.M., Searle, M.P., Waters, D.J., Horstwood, M.S.A., Parrish, R.R., 2012. Combined thermobarometry and geochronology of peraluminous metapelites from the Karakoram metamorphic complex, North Pakistan; new insight into the tectonothermal evolution of the Baltoro and Hunza Valley regions. J. Metamorph. Geol. 30, 793–820.
Peltzer, G., Tapponnier, P., 1988. Formation and evolution of strike-slip faults, rifts and basins during the India–Asia collision: an experimental approach. J. Geophys. Res. 93, 15085–15117.
Phillips, R.J., 2008. Geological map of the Karakoram fault zone, Eastern Karakoram, Ladakh, NW Himalaya. J. Maps 2008, 21–37.
Phillips, R.J., Searle, M.P., 2007. Macrostructural and microstructural architecture of the Karakoram fault: relationship between magmatism and strike-slip faulting. Tectonics 26, TC3017.
Phillips, R.J., Parrish, R.R., Searle, M.P., 2004. Age constraints on ductile deformation and long-term slip rates along the Karakoram fault zone, Ladakh. Earth Planet. Sci. Lett. 226, 305–319.
Phillips, R.J., Searle, M.P., Parrish, R.R., 2013. The geochemical and temporal evolution of the continental lithosphere and its relationship to continental-scale faulting: the Karakoram Fault, eastern Karakoram, NW Himalayas. Geochem. Geophys. Geosyst. 14, 583–603.
Powell, R., 1978. Equilibrium Thermodynamics in Petrology an IntroductionHarper and Row Ltd., London p. 284.
Pullen, A., Kapp, P., Gehrels, G.E., Ding, L., Zhang, Q.H., 2011. Metamorphic rocks in central Tibet: lateral variations and implications for crustal structure. Geol. Soc. Am. Bull. 123, 585–600.
Reichardt, H., Weinberg, R.F., 2012. Hornblende chemistry in meta- and diatexites and its retention in the source of leucogranites: an example from the Karakoram Shear Zone, NW India. J. Petrol. 53, 1287–1318.
Reichardt, H., Weinberg, R.F., Andersson, U.B., Fanning, C.M., 2010. Hybridization of granitic magmas in the source: the origin of the Karakoram Batholith, Ladakh, NW India. Lithos 116, 249–272.
Robinson, A.C., 2009. Geologic offsets across the Karakoram Fault: implications for its role and terrane correlations in the western Himalayan–Tibetan orogen. Earth Planet. Sci. Lett. 279, 123–130.
Rolland, Y., Pêcher, A., 2001. The Pangong granulites of the Karakoram Fault (Western Tibet): vertical extrusion within a lithosphere-scale fault? Earth Planet. Sci. 332, 363–370.
Rolland, Y., Mahéo, G., Pêcher, A., Villa, I.M., 2009. Syn-kinematic emplacement of the Pangong metamorphic and magmatic complex along the Karakorum fault (N Ladakh). J. Asian Earth Sci. 34, 10–25.
Rutter, E.H., Faulkner, D.R., Brodie, K.H., Phillips, R.J., Searle, M.P., 2007. Rock deformation processes in the Karakoram fault zone, Ladakh, NW India. J. Struct. Geol. 29, 1315–1326.
Searle, M.P., 1996. Geological evidence against large-scale pre-Holocene offsets along the Karakoram Fault: implications for the limited extrusion of the Tibetan Plateau. Tectonics 15, 171–186.
Searle, M.P., 2013. Crustal melting, ductile flow, and deformation in mountain belts: cause and effect relationships. Lithosphere 5, 547–554.
Searle, M.P., Phillips, R.J., 2007. Relationships between right-lateral shear along the Karakoram Fault and metamorphism, magmatism, exhumation and uplift: evidence from the K2, Gasherbrum and Pangong ranges, north Pakistan and Ladakh. J. Geol. Soc. Lond. 164, 439–450.

Searle, M.P., Weinberg, R.F., Dunlap, W.J., 1998. Transpressional tectonics along the Karakoram fault zone, northern Ladakh: constraints on Tibetan extrusion. Geol. Soc. Lond., Spec. Publ. 135, 307–326.

Searle, M.P., Parrish, R.R., Thow, A.V., Noble, S.R., Phillips, R.J., Waters, D.J., 2010. Anatomy, age and evolution of a collisional mountain belt: the Baltoro granite batholith and Karakoram Metamorphic Complex, Pakistani Karakoram. J. Geol. Soc. Lond. 167, 183–202.

Searle, M.P., Elliott, J.R., Phillips, R.J., Chung, S.-L., 2011. Crustal-lithospheric structure and continental extrusion of Tibet. J. Geol. Soc. Lond. 168, 633–672.

Stipp, M., Stünitz, H., Heilbronner, R., Schmid, S.M., 2002. Dynamic recrystallization of quartz: correlation between natural and experimental conditions. Geol. Soc. Lond., Spec. Publ. 200, 171–190.

Streule, M.J., Phillips, R.J., Searle, M.P., Waters, D.J., Horstwood, M.S.A., 2009. Evolution and chronology of the Pangong Metamorphic Complex adjacent to the Karakoram Fault, Ladakh: constraints from thermobarometry metamorphic modelling and U–Pb geochronology. J. Geol. Soc. Lond. 166, 919–932.

Thanh, N.X., Sajeev, K., Itaya, T., Windley, B.F., 2011. Multiple garnet growth in garnet–kyanite–staurolite gneiss, Pangong metamorphic complex, Ladakh Himalaya: new constraints on tectonic setting. Lithos 127, 552–563.

Tullis, J., Yund, R.A., 1985. Dynamic recrystallization of feldspar: a mechanism for ductile shear zone formation. Geology 13, 238–241.

Valli, F., Leloup, P.H., Paquette, J.L., Arnaud, N., Li, H.B., Tapponnier, P., Lacassin, R., Guillot, S., Lui, D.Y., Deloule, E., Xu, Z.Q., Mahéo, G., 2008. New U–Th/Pb constraints on timing of shearing and long-term slip-rate on the Karakorum fault. Tectonics 27, TC5007.

Villa, I.M., Lemennicier, Y., Le Fort, P., 1996. Late Miocene to Early Pliocene tectonometamorphism and cooling in south-central Karakorum and Indua–Tsangpo suture, Chogo Lungma area (NE Pakistan). Tectonophysics 260, 201–214.

Wallis, D., Phillips, R.J., Lloyd, G.E., 2013. Fault weakening across the frictional–viscous transition zone, Karakoram Fault Zone, NW Himalaya. Tectonics. http://dx.doi.org/10.1002/tect.20076.

Wang, S., Wang, E., Fang, X., Lai, Q., 2011. U–Pb SHRIMP and $^{40}Ar/^{39}Ar$ ages constrain the deformation history of the Karakoram fault zone (KFZ), SW Tibet. Tectonophysics 509, 208–217.

Wang, S., Wang, C., Phillips, R.J., Murphy, M.A., Fang, X., Yue, Y., 2012. Displacement along the Karakoram fault, NW Himalaya, estimated from LA-ICP-MS U–Pb dating of offset geologic markers. Earth Planet. Sci. Lett. 337, 156–163.

Wang, S., Mo, Y., Phillips, R.J., Wang, C., 2013a. Karakoram fault activity defined by temporal constraints on the Ayi Shan detachment, SW Tibet. Int. Geol. Rev. http://dx.doi.org/10.1080/00206814.2013.818750.

Wang, S., Murphy, M.A., Phillips, R.J., Wang, C., 2013b. Reply to comment on "Displacement along the Karakoram fault, NW Himalaya, estimated from LA-ICP-MS U–Pb dating of offset geologic markers" by Leloup et al. in EPSL, 2013. Earth Planet. Sci. Lett. 363, 246–248.

Weinberg, R.F., Searle, M.P., 1998. The Pangong Injection Complex, Indian Karakoram: a case of pervasive granite flow through hot viscous crust. J. Geol. Soc. Lond. 155, 883–891.

Weinberg, R.F., Mark, G., Reichardt, H., 2009. Magma ponding in the Karakoram shear zone, Ladakh, NW India. Geol. Soc. Am. Bull. 121, 278–285.

Weller, O.M., St-Onge, M.R., Waters, D.J., Rayner, N., Searle, M.P., Chung, S.-L., Palin, R.M., Lee, Y.-H., Xu, X., 2013. Quantifying Barrovian metamorphism in the Danba Structural Culmination of eastern Tibet. J. Metamorph. Geol. 31, 909–935.

Wyllie, P.J., 1977. Crustal anatexis: an experimental review. Tectonophysics 43, 41–71.

Zhang, K.-J., Cai, J.-X., Zhang, Y.-X., Zhao, T.-P., 2006. Eclogites from central Qiangtang, northern Tibet (China) and tectonic implications. Earth Planet. Sci. Lett. 245, 722–729.